Radiative Transport in Toroidal Plasmas

Satish Puri

IPP 4/273 October 1996

MAX-PLANCK-INSTITUT FÜR PLASMAPHYSIK

85748 GARCHING BEI MÜNCHEN

MAX-PLANCK-INSTITUT FÜR PLASMAPHYSIK

GARCHING BEI MÜNCHEN

Radiative Transport in Toroidal Plasmas

Satish Puri

IPP 4/273 October 1996

Die nachstehende Arbeit wurde im Rahmen des Vertrages zwischen dem Max-Planck-Institut für Plasmaphysik und der Europäischen Atomgemeinschaft über die Zusammenarbeit auf dem Gebiete der Plasmaphysik durchgeführt.

Radiative transport in toroidal plasmas

Satish Puri

Max-Planck-Institut für Plasmaphysik, 85748 Garching, Germany

ABSTRACT

Momentum transfer via Kirchhoff radiation of electrostatic electron and ion-cyclotron-harmonic waves contributes an enhanced collisionality far in excess of that given by the Fokker-Planck term in the existing neoclassical models. The resultant particle and thermal transport resembles the observed anomalous transport in ohmically heated toroidal plasmas.

PACS: 52.25.Fi, 52.55.-s, 52.55.Dy, 52.55.Fa, 52.55.Hc

Particle and thermal transport in toroidal plasmas greatly exceeds the neoclassical predictions based on two-particle collisional encounters included in the Fokker-Planck term of the Vlasov-Boltzmann equation. The search for an explanation of this anomalous behavior constitutes "an outstanding physics conundrum of the late 20th century."[1] The solution to this dilemma is sought in non-collisional terms, notably via non-linear turbulent interactions[2]; there is evidence supporting turbulent transport near the plasma edge as well as in the plasma core prior to stabilization through reversed shear. A quarter century of theoretical, computational and experimental work has yielded many other valuable insights; but the enigma persists.

In addition to the two-body collisional encounters, particles in a plasma are capable of exchanging momentum with waves; the principle is exploited in radio-frequency current-drive experiments. Since particles also radiate waves in a thermal plasma (Kirchhoff radiation), another mode of momentum exchange among the particles in a plasma is possible via the emission and absorption of radiation.[3]

In this Letter it is shown that the collisionality occurring via the collective process of radiative momentum exchange far exceeds that due to the Fokker-Planck encounters. The resultant thermal and particle transport parallels the experimentally observed behavior. Since this enhanced collisional transport resembles, yet transcends the neoclassical projections, it will be referred to as *supraclassical transport.*

The decay rate of energy of a wave of the form $\sim \exp[i(\mathbf{k}\cdot\mathbf{r}-\omega t)]$ is given by $2\Im[\omega]$, where $\Im[\omega]$ is the imaginary part of ω. Multiplication with the energy density $T\,d\mathbf{k}/(2\pi)^3$ of cavity modes in the phase-space volume element $d\mathbf{k}$ gives the total radiated power density (assuming thermodynamic equilibrium)

$$\eta_E = \frac{2T}{(2\pi)^3}\int_{\mathbf{k}} \Im[\omega]\; d\mathbf{k}\;, \tag{1}$$

where T is the temperature in energy units. Radiation decreases particle velocities such that $<(\Delta v)^2> \sim \eta_E$, while reabsorption restores $<(\Delta v)^2>$ by an identical amount in thermal equilibrium. Rayleigh-Jeans approximation of Planck's formula is used in the derivation of Kirchhoff's law in (1). Several alternative forms of Kirchhoff's

law occur in the literature.[4,5] Since the photon of energy $\hbar\omega$ carries a parallel (to the ambient magnetic-field direction) momentum $\hbar k_\parallel$, the intensity of the radiated parallel-momentum density may be expressed as

$$\eta_{\mu_\parallel} = \frac{2T}{(2\pi)^3} \int_{\mathbf{k}} \frac{k_\parallel}{\Re[\omega]} \Im[\omega] \, d\mathbf{k} \, , \tag{2}$$

$\Re[\omega]$ being the real part of ω. $\Im[\omega]$ in Eq.(2) is comprised of contributions $\Im[\omega^\sigma]$ from all the particle species σ such that $\sum_\sigma \Im[\omega^\sigma] = \Im[\omega]$. The parallel momentum emitted per second by the species σ at the wavenumber $\mathbf{k}(\omega)$ is given by

$$\eta^\sigma_{\mu_\parallel}(\mathbf{k}) = \frac{2T}{(2\pi)^3} \frac{k_\parallel}{\Re[\omega]} \Im[\omega^\sigma] \, . \tag{3}$$

Thermal emission implies that $\eta^\sigma_{\mu_\parallel}(\mathbf{k})$ is of the form $\sim m_\sigma < (\Delta v_\parallel)^2 > / v_{p\parallel}$, where $v_{p\parallel} = \omega/k_\parallel$ is the parallel-phase-velocity of the wave. A fraction $\Im[\omega^\xi]/\Im[\omega]$ of this momentum is absorbed by the species ξ. The momentum-transfer rate from species σ to ξ (and vice versa) at the wavenumber $\mathbf{k}$ becomes

$$\eta^{\sigma\xi}_{\mu_\parallel}(\mathbf{k}) = \frac{2T}{(2\pi)^3} \frac{k_\parallel}{\Re[\omega]} \frac{\Im[\omega^\sigma]\Im[\omega^\xi]}{\Im[\omega]} \, . \tag{4}$$

Dividing $\eta^{\sigma\xi}_{\mu_\parallel}(\mathbf{k})$ by the particle's parallel momentum $m_\sigma v_{\parallel\sigma}$ gives the *total* number of collisions per second occurring at the wavenumber $\mathbf{k}$ as

$$\nu^{rad}_{\sigma\xi}(\mathbf{k}) = \left| \eta^{\sigma\xi}_{\mu_\parallel}(\mathbf{k}) / m_\sigma v_{\parallel\sigma} \right| \, , \tag{5}$$

where m_σ is the particle mass and $v_{\parallel\sigma}$ is the particle's parallel velocity defined in Eq.(7). Attempt is under way to put the heuristic derivation of Eq.(5) from Eq.(4) on a firmer basis using the Balescu-Lenard equation; the plausibility of the present derivation is supported by the agreement of these findings with the experimental results.

Dividing $\nu^{rad}_{\sigma\xi}(\mathbf{k})$ by the particle density n_σ and integrating over $\mathbf{k}$ gives the radiation-induced collision frequency *per particle* relevant for toroidal transport ($\sigma \equiv \xi$ for self collisions)

$$\nu^{rad}_{\sigma\xi} = \frac{T}{\pi^2 n_\sigma} \int_0^{\alpha_D k_D} \int_0^{\alpha_D k_D} \left| \frac{1}{m_\sigma v_{\parallel\sigma}} \frac{\Im[\omega^\sigma]\Im[\omega^\xi]}{\Re[\omega]\Im[\omega]} \right| k_\parallel k_\perp \, dk_\parallel dk_\perp \, , \tag{6}$$

In deriving Eq.(6), it is assumed that positive and negative $k_\parallel$ contribute equally to ν^{rad}. The k integrations extend up to $\alpha_D k_D$, where $k_D = 2\pi/\lambda_D$ is the Debye wavenumber corresponding to the Debye length

$$\lambda_D = \left(\sum_\sigma \frac{n_\sigma q_\sigma^2}{T_\sigma} \right)^{-1/2} , \tag{7}$$

q_σ is the charge carried by the species σ particles and $\alpha_D \sim \mathcal{O}(1)$. The precise value of α_D defines the small-wavelength limit for the applicability of the Vlasov-Boltzmann equation.

The density of cavity modes clusters at the larger $|\mathbf{k}|$ values (reminiscent of the ultraviolet catastrophe) making the small-wavelength, large-$|\mathbf{k}|$, electrostatic-cyclotron-harmonic modes the prime contributors to ν^{rad} in Eq.(6). These highly-damped modes are the large-$k_\parallel$ extensions of the Bernstein[6] modes. For $k_\parallel > \omega/v_{te}$ (v_t is the particle thermal velocity), the ionic branch is called the electrostatic-ion-cyclotron wave[7]. The wave absorption/emission occurs via Landau and cyclotron damping.

For a given $\mathbf{k}(\omega)$, $\Im[\omega^\sigma]$ for each of the particle species consists of contributions from all the cyclotron-harmonic numbers n, such that $\Im[\omega^\sigma] = \sum_n \Im[\omega^\sigma]_n$. The corresponding particle parallel velocities in Eq.(6) are given by the relation

$$\omega - n\omega_{c\sigma} - k_\parallel v_{\parallel\sigma} = 0 . \tag{8}$$

Since regions of strongest absorption correspond to large $k_\parallel$ and small $\omega - n\omega_{c\sigma}$, the largest collisionality contributions occur for the low-parallel-velocity (trapped-particle) population. The set of $\Im[\omega^\sigma]_n$ are obtained using the complete, homogeneous hot-plasma, cylindrical-geometry, non-relativistic dispersion relation[8] $D(\omega, \mathbf{k}) = 0$.

Equation (6) shows that, in contrast to the neoclassical case, the $\nu_{ei}^{rad}/\nu_{ie}^{rad}$ ratio for a given $\mathbf{k}(\omega)$ and $T_e = T_i$ scales as $(m_i/m_e)(v_{\parallel i}/v_{\parallel e})$. For the ion-cyclotron-harmonic waves the electrons are Landau damped ($n = 0$), whereas the ions undergo cyclotron-harmonic damping ($n \neq 0$), one obtains from Eq.(8), $v_{\parallel i}/v_{\parallel e} \sim \mathcal{O}(1 - n\omega_{ci}/\omega)$. Thus, $\nu_{ei}^{rad}/\nu_{ie}^{rad} \sim (m_i/m_e)(1 - n\omega_{ci}/\omega)$ for the nth ion-cyclotron harmonic component. Hence, supraclassical transport is not intrinsically ambipolar (typically ν_{ei}^{rad} exceeds ν_{ie}^{rad}

by a factor of only about 50 in an electron-proton plasma); a radially inward-directed electric field is needed to maintain ambipolarity. Such an electric field and the attendant plasma rotation are a hallmark of tokamak plasmas.

Unless otherwise stated, it is assumed that $T_e = T_i = T$, atomic mass $A = 1$ and $\alpha_D = 1$ in the following computational results for a two-component, electron-ion plasma in thermodynamic equilibrium. One hundred cyclotron harmonics are included in the integration of Eq.(6).

Figure 1 shows the computed radiative collision frequencies as a function of the toroidal magnetic field. ν_{ee}^{rad} increases linearly with B_0 while ν_{ei}^{rad}, ν_{ie}^{rad} and ν_{ii}^{rad} exhibit a quadratic dependence on B_0. The resultant diffusivities (to the lowest approximation, ignoring off-diagonal terms) scale as $\chi_e \sim B_0^{-1}$ and $\chi_i \sim B_0^0$. ν_{ee}^{rad} is almost twenty times larger than the corresponding Fokker-Planck value. This discrepancy becomes still more pronounced at lower plasma densities, up to one hundred times the neoclassical value. *The enhancement in χ_e is at the core of the transport riddle; its resolution alone establishes the importance of radiative collisionality.* For $B_0 \sim 2T$, $\nu_{ee}^{rad}/\nu_{ii}^{rad} \sim m_i/m_e$, so that electrons and ions become equal participants in thermal conduction. χ_e dominates energy transport below $B_0 \sim 2T$ and χ_i above $B_0 \sim 2T$.

With increasing B_0, the smallest permissible perpendicular wavelength $\mathcal{O}(\lambda_D)$ comes nearer in value to the much larger ion gyroradius causing a more intense interaction of the waves with the ions. The effect is weaker for electrons because their gyroradius is already close to the Debye length.

An increase in the ion gyroradius for higher atomic mass number A results in a weakened wave-ion interaction and $\nu_{ii}^{rad}, \nu_{ie}^{rad} \sim A^{-3/2}$ (Fig.2), leading to a $A^{1/2}$ isotope mass dependence of ion energy containment time.[9] A, however, has no direct influence on electron heat transport; the isotope mass effect on χ would be weak in low-field ($B_0 \lesssim 2T$) tori. Since the Landau damping of electrons in the electrostatic ion-cyclotron-harmonic waves remains unaffected by A, ν_{ei}^{rad} decreases only as $A^{-1/2}$. The particle containment time response to A is a mixture of a favorable ν_{ie} scaling and

an unfavorable ν_{ei} scaling.

Figure 3 shows that the temperature dependence of radiative collisions follows the neoclassical $T^{-3/2}$ dependence. This behavior may be inferred from Eq.(6) where $\nu^{rad} \sim k_D^4 v_t \sim T^{-3/2}$ (the Debye length to gyroradius ratio remaining constant).

An inspection of Eq.(6) would indicate a linear dependence of ν^{rad} on n_e due to the n_e^2 variation of k_D^4. However, the simultaneous shift of λ_D away from the gyroradius offsets the gain in ν^{rad} due to the density increase. This is most pronounced for ions whose gyroradius is already well in excess of the Debye length. Figure 4 shows that $\nu_{ee}^{rad} \sim n_e^{0.6}$, $\nu_{ei}^{rad} \sim n_e^0$ while $\nu_{ii}^{rad} \sim n_i^{0.1}$. The crossover of ν_{ei}^{rad} and ν_{ei}^{nc} occurs at a density of $n_e \sim 6 \times 10^{19}\, m^{-3}$. Below these densities, the electron and ion populations are uncoupled[9] so that the Debye length is determined by the colder ion population. The low value of λ_D with a correspondingly larger integration limit in Eq.(6) would lead to larger collisionalities than those appearing in Fig.4. The combined effect of ν_{ei} crossover and the electron-ion thermal coupling may be responsible for the linear (LOC) and saturated (SOC) ohmic confinement regimes[9]. At higher values of B_0, and with the accompanying higher plasma temperatures, both the ν_{ei} crossover and the electron-ion thermal coupling shift to higher densities, in accord with observations.[9] Conversely, for lower B_0, the LOC-SOC transition occurs at lower densities. Higher isotope mass results in poorer electron-ion coupling pushing the LOC-SOC transition to higher densities as observed experimentally[10]. The ν_{ii}^{rad}, ν_{ii}^{nc} crossover occurs at a somewhat higher density, $n_e \sim 10^{20}\, m^{-3}$. The electron-electron radiative collisionality ν_{ee}^{rad}, on the other hand, continues to dominate over the neoclassical value ($\nu_{ee}^{nc} \approx \nu_{ei}^{nc}$) for densities as high as $n_e \sim 10^{23}\, m^{-3}$.

Figure 5, showing the velocity distributions of the colliding particles, confirms that the bulk of the collisions is contributed by the trapped particles. Hence the enhancement in the electron-ion collisionality does not affect the Spitzer resistivity.

Figure 6 shows the extreme sensitivity of radiative collisionality to Debye length. Thus a fourfold increase in α_D causes ν_{ee}^{rad} to grow by almost two orders of magni-

tude. A careful comparison of the supraclassical theory with the experimental data would allow an accurate determination of α_D and thereby settle a long-standing uncertainty regarding the low-wavelength limit for the applicability of the Vlasov-Boltzmann equation.

The above findings would profoundly influence our thinking regarding bootstrap current, radio-frequency current drive, profile consistency, and the interpretation of a host of radio-frequency and neutral-beam heating experiments.

As an example, consider the problem of low-phase-velocity Alfven-wave current drive in a tokamak plasma. According to the current projections based on neoclassical theory, momentum given primarily to the trapped electrons via Landau damping is transferred to the ions through the plasma rotation arising from the radial electric field caused by the Ware[11] pinch of the trapped electrons.[12] If F^p and F^b are the forces driving the passing and the banana particles, respectively, the resultant current drive is given by

$$j \approx -\frac{e}{m\nu_{ei}}\left[F^p + \frac{m_e}{m_i}\left(\frac{\nu_{ei}+\nu_{ee}}{\nu_{ii}}\right)F^b\right] . \tag{9}$$

In the neoclassical picture with $\nu_{ei} \approx \nu_{ee} \approx \sqrt{m_i/m_e}\,\nu_{ii}$, the effectiveness of F^b is a mere $\sqrt{m_e/m_i}$ that of F^p in driving toroidal plasma current. For the supraclassical case, on the other hand, $\nu_{ee}^{rad}/\nu_{ei}^{rad} \sim \mathcal{O}(\sqrt{m_i/m_e})$ and $\nu_{ee}^{rad}/\nu_{ii}^{rad} \sim \mathcal{O}(m_i/m_e)$; F^b and F^p become equally effective in the current-drive process. The momentum given to the trapped particles is rapidly transferred to the entire electron population giving rise to a normalized Alfven-wave current-drive efficiency of $\gamma \approx 1\,AW^{-1}m^{-2}$ which is in fortuitous agreement with the earlier results[13,14] that ignore the plasma rotation resulting from the electron Ware pinch.

In addition to radiative collisionality by the emission and absorption of parallel momentum, direct transfer of radiative energy also takes place.[4,5,15] In the present context, however, such direct transport is insignificant.[15]

According to Eq.(1), the total radiated power per unit volume by the electron and ion components is $\sim 10^3\,GWm^{-3}$ and $\sim 50\,MWm^{-3}$, respectively. However, reab-

sorption within picoseconds results in a net energy density

$$U = \frac{T}{(2\pi)^3} \int_{\mathbf{k}} d\mathbf{k} \,, \tag{10}$$

of only $\sim 20\, mWm^{-3}$, much too low to be detected experimentally. The parallel-momentum density $\sim 10^3\, Nm^{-3}$ radiated per second by electrons as given by Eq.(2) accords with the enhanced ν_{ee}^{rad}. Ions, in contrast, radiate only $\sim 1\, Nm^{-3}$ parallel-momentum density per second.

The results of this Letter are strictly applicable only for plasmas in thermodynamic equilibrium. Significant deviations from Maxwellian velocity distributions in auxiliary heated plasmas require separate treatment. In a similar vein, the present results are inapplicable to the improved confinement observed in reversed shear, non-thermal (steady-state does not imply thermal equilibrium) experiments. Furthermore, non-equilibrium as well as quasi-equilibrium plasmas with free energy sources residing in plasma and magnetic-field inhomogeneities, are subject to a vast array of transport processes including plasma turbulence. The present results, therefore, define the minimum irreducible limit of toroidal transport in ohmically-heated plasmas near thermal equilibrium.

In summary, radiative collisionality is able to resolve some of the perplexing dilemmas of toroidal transport; namely, (i) enhanced electron thermal conduction, (ii) magnetic-field dependence, (iii) isotope mass dependence, (iv) the origin of the radial electric field and plasma rotation in ohmic discharges, and perhaps (v) the cause behind the linear (LOC) and saturated (SOC) confinement regimes. Radiative collisionality also provides insights into diverse phenomena dependent upon plasma transport.

Although this Letter is devoted to toroidal plasma confinement objectives, the findings of enhanced transport across inhomogeneous magnetic fields has significance for astrophysical and cosmic plasmas as well.

I am thankful to Profs. F. Wagner and R. Wilhelm for helpful comments during the preperation of the manuscript and to Prof. D. Pfirsch for pointing out the possibility of using the Balescu-Lenard equation.

References

[1] J. D. Callen, Phys. Fluids B **4**, 2142 (1992).

[2] B. B. Kadomtsev, in *Plasma Turbulence*, Academic Press, London (1965).

[3] S. Puri, in *Proceedings of the 22nd European Conference on Controlled Fusion and Plasma Physics, Bournemouth*, 1995 (European Physical Society, Petit-Lancy, Switzerland, 1995), Volume. 19C, p.197.

[4] G. Bekefi, in *Radiation Processes in Plasmas*, John-Wiley, New York(1966).

[5] M. Bornatici, et al., Nuclear Fusion **9**, 1153(1983).

[6] I. B. Bernstein, Phys. Rev. **109**, 10(1958).

[7] N. D'Angelo and R. W. Motley, Phys. Fluids **5**, 633(1962).

[8] T. H. Stix, in *Waves in Plasmas*, AIP, New York(1992).

[9] F. Wagner and U. Stroth, Plasma Phys. Control. Fusion **35**, 1321(1993).

[10] E. Simmet, private communication.

[11] A. A. Ware, Phys. Rev. Lett. **25**, 15(1970).

[12] Y. Kolesnichenko, V. Parail, and G. Pereverzev, in *Reviews of Plasma Physics*, edited by B. B. Kadomtsev (Consultants Bureau, New York, 1992), Vol.17.

[13] A. G. Elfimov and S. Puri, Nucl. Fusion **30**, 1215(1990).

[14] S. Puri, in *Proceedings of the IAEA Technical Committee Meeting on Fast Wave Current Drive in Reactor Scale Tokamaks, Arles*, 1991 (Association EURATOM-CEA sur la Fusion, Cadarache, France, 1991), p.200.

[15] S. Puri, in *Proceedings of the 17th European Conference on Controlled Fusion and Plasma Heating, Amsterdam*, 1990 (European Physical Society, Petit-Lancy, Switzerland, 1990), Volume 14B, p.1770.

Figure captions

Fig.1 ν^{rad} versus B_0 ($n_e = 10^{20}\, m^{-3}$, $T = 10\, keV$).

Fig.2 ν^{rad} versus atomic mass A ($n_e = 10^{20}\, m^{-3}$, $T = 10\, keV$, $B_0 = 6\, T$). Half-integer values of A are included to improve the definition of the curves.

Fig.3 ν^{rad} versus T ($n_e = 10^{20}\, m^{-3}$, $B_0 = 6\, T$).

Fig.4 ν^{rad} (solid lines) and ν^{nc} (dashed lines) versus n_e ($T = 10\, keV$, $B_0 = 6\, T$).

Fig.5 Velocity distribution of colliding particles ($n_e = 10^{20}\, m^{-3}$, $T = 10\, keV$, $B_0 = 6\, T$).

Fig.6 ν^{rad} versus α_D ($n_e = 10^{20}\, m^{-3}$, $T = 10\, keV$, $B_0 = 6\, T$).

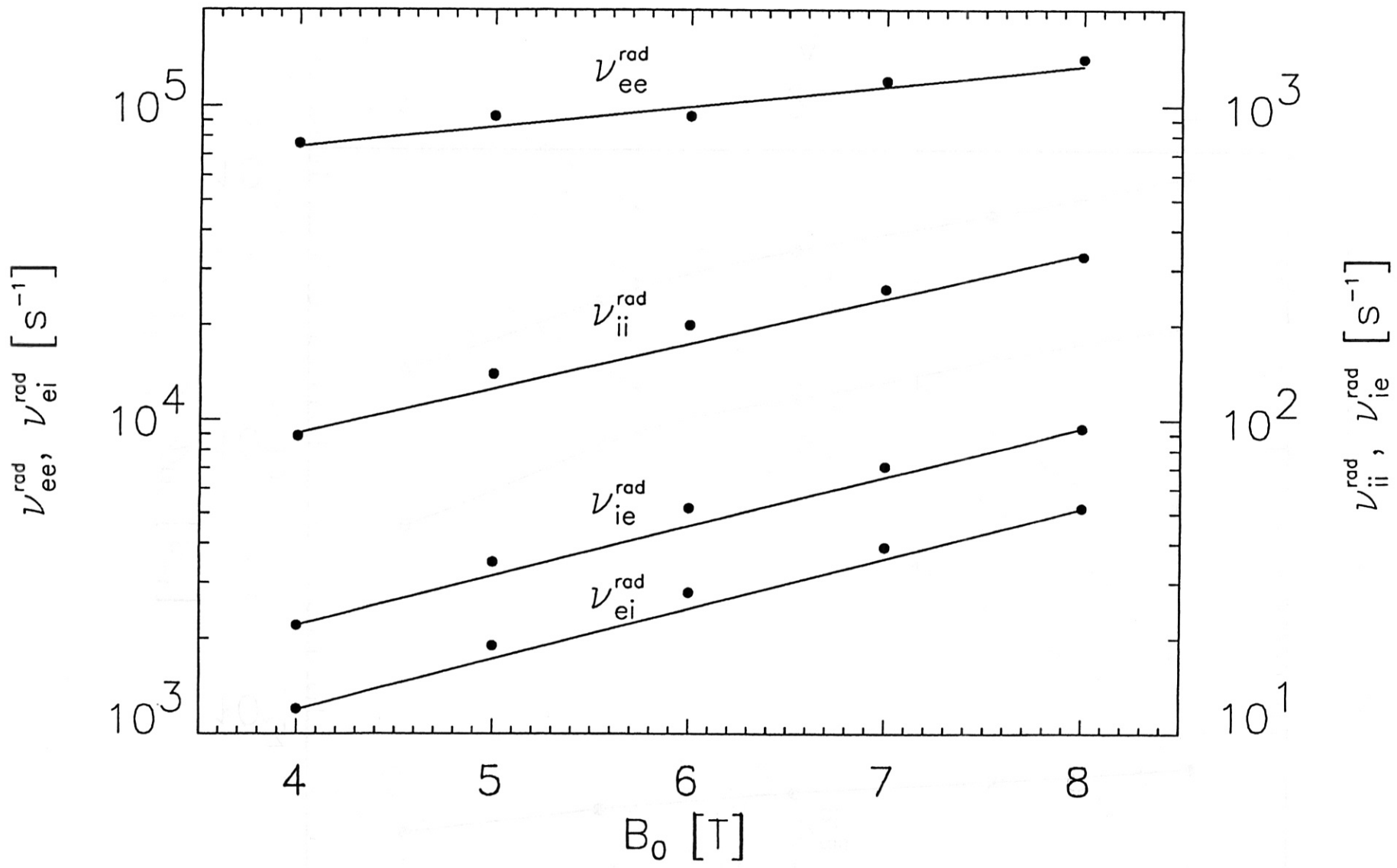
ν_{ee}^{rad}
ν_{ii}^{rad}
ν_{ie}^{rad}
ν_{ei}^{rad}
10^5
10^4
10^3
10^3
10^2
10^1
4
5
6
7
8
B_0 [T]
ν_{ee}^{rad}, ν_{ei}^{rad} [s^{-1}]
ν_{ii}^{rad}, ν_{ie}^{rad} [s^{-1}]

FIG. 1

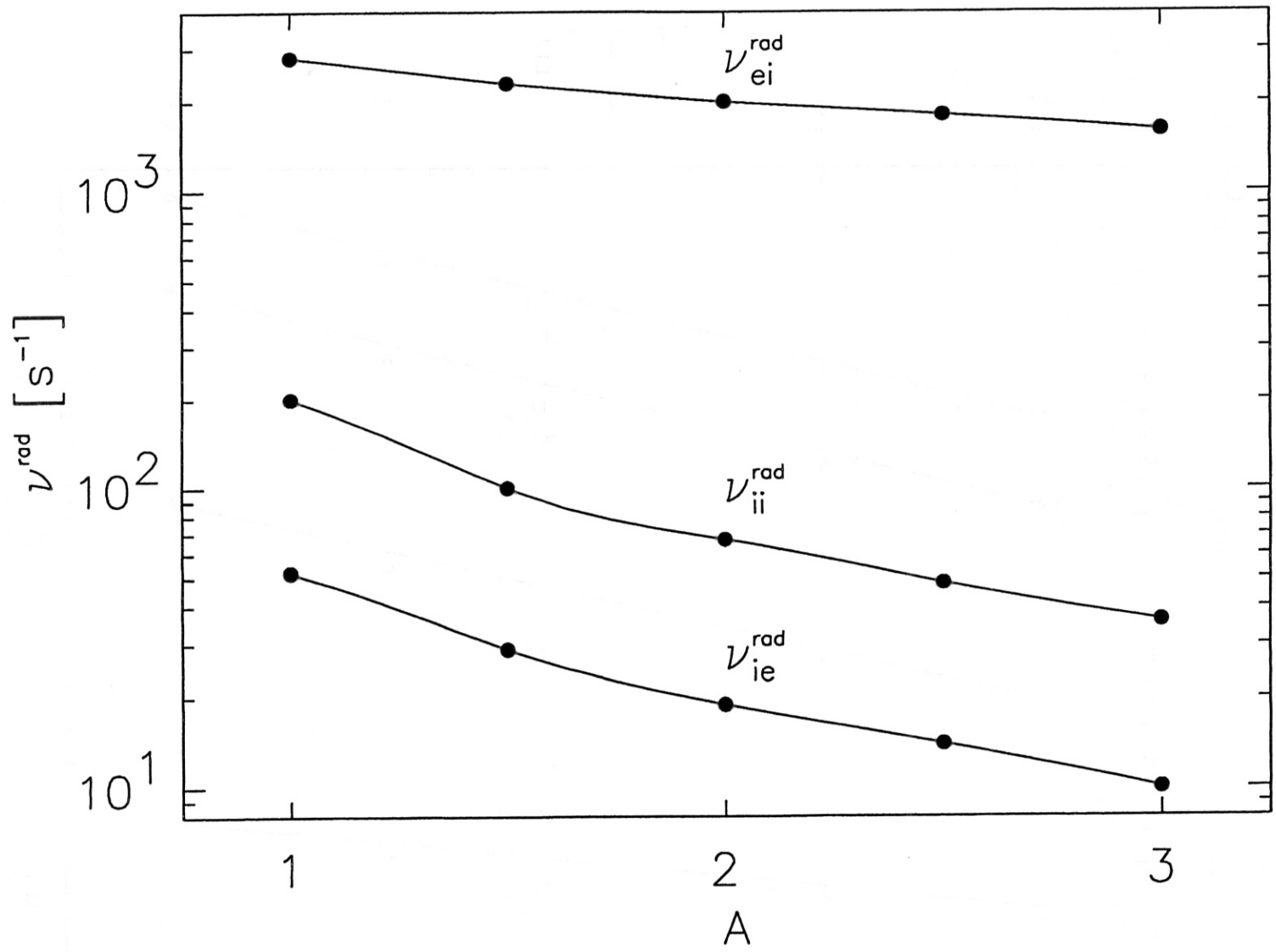

FIG. 2

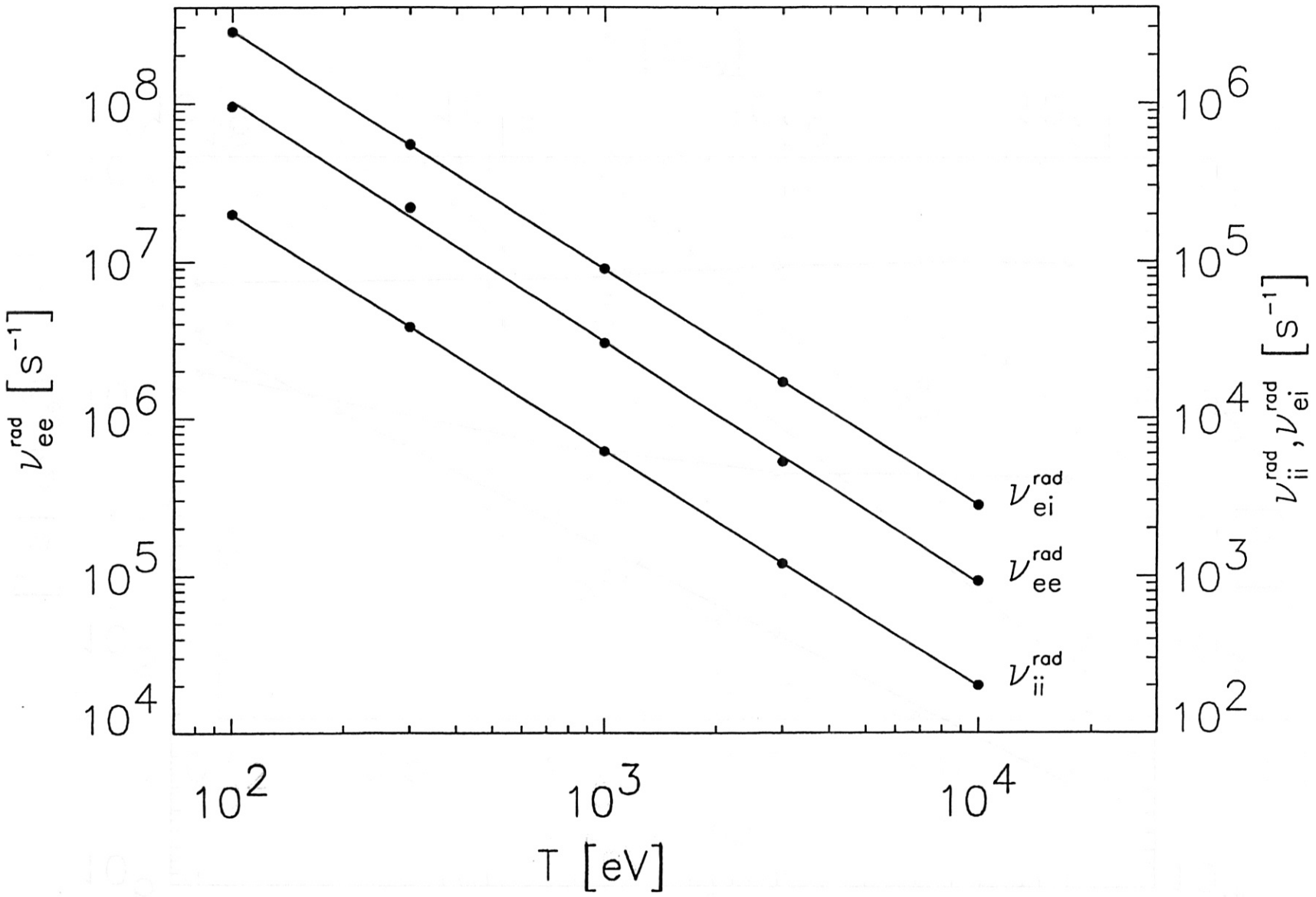
10^8
10^7
10^6
10^5
10^4
ν_{ee}^{rad} [s^{-1}]
10^6
10^5
10^4
10^3
10^2
ν_{ii}^{rad}, ν_{ei}^{rad} [s^{-1}]
ν_{ei}^{rad}
ν_{ee}^{rad}
ν_{ii}^{rad}
10^2
10^3
10^4
T [eV]

FIG. 3

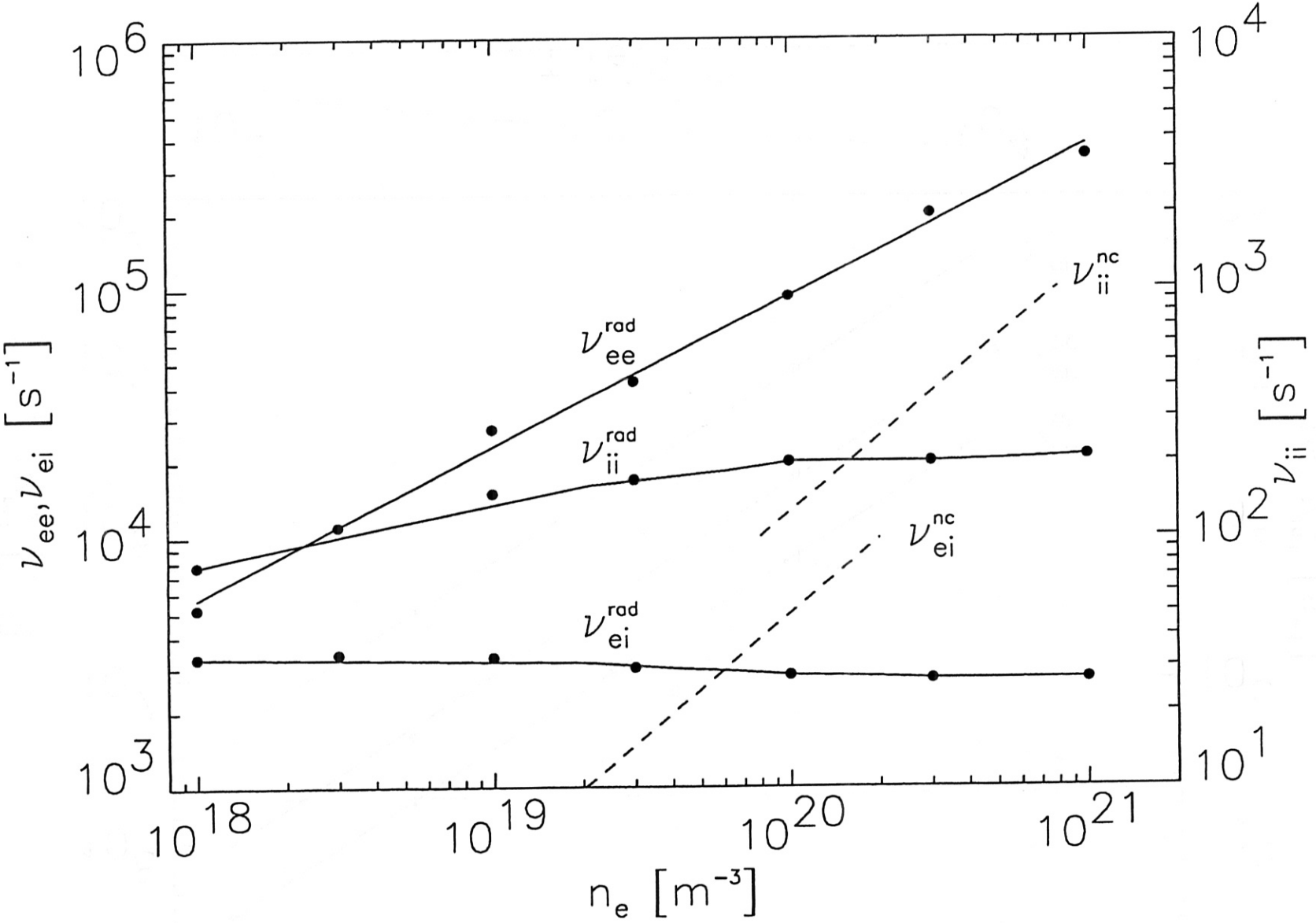
10^6
10^5
10^4
10^3
10^4
10^3
10^2
10^1
ν_{ee}, ν_{ei} [s^{-1}]
ν_{ii} [s^{-1}]
ν_{ee}^{rad}
ν_{ii}^{rad}
ν_{ei}^{rad}
ν_{ii}^{nc}
ν_{ei}^{nc}
10^{18}
10^{19}
10^{20}
10^{21}
n_e [m^{-3}]

FIG. 4

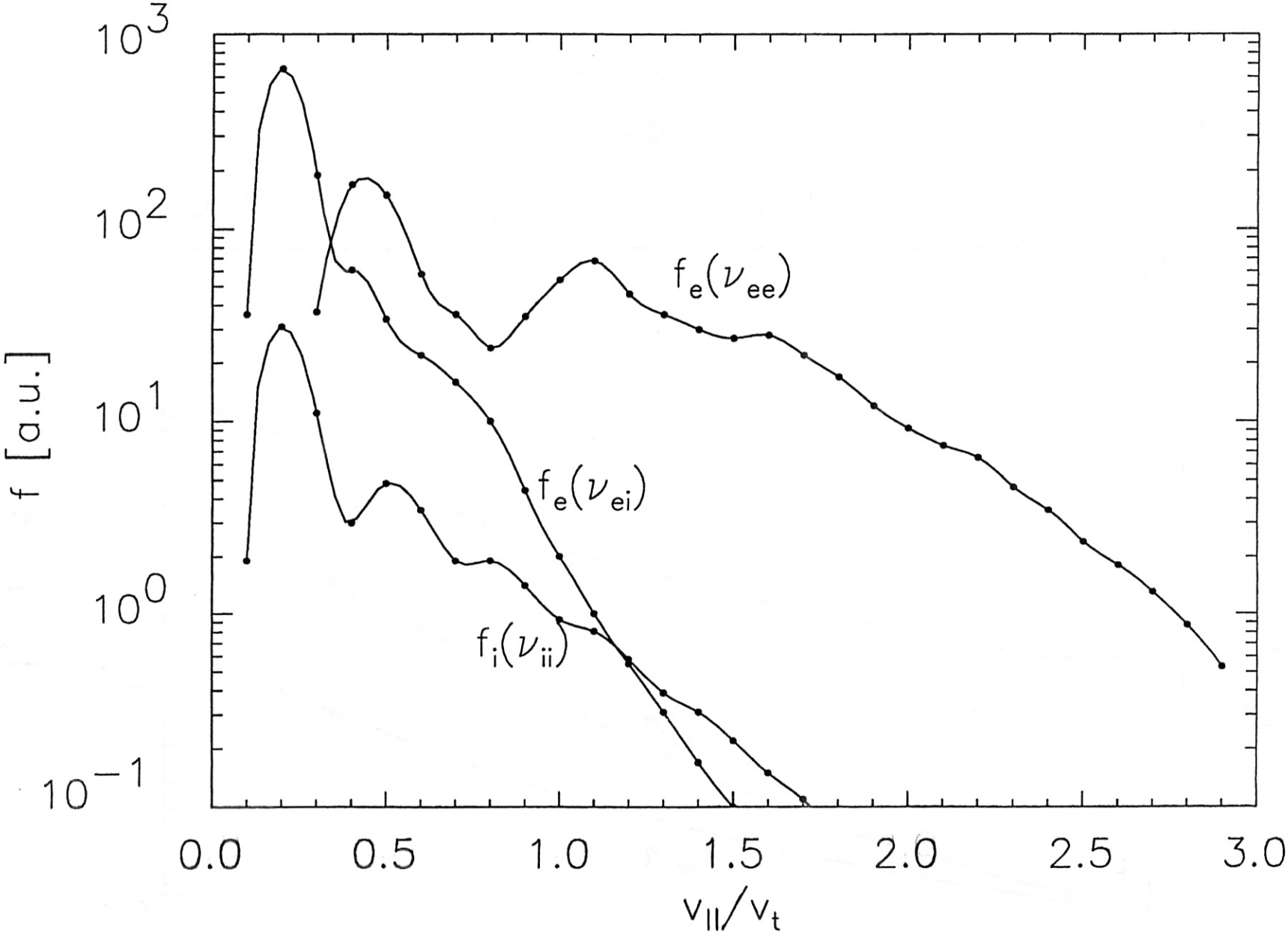
10^3
10^2
10^1
10^0
10^{-1}
f [a.u.]
$f_e(\nu_{ee})$
$f_e(\nu_{ei})$
$f_i(\nu_{ii})$
0.0
0.5
1.0
1.5
2.0
2.5
3.0
$v_{||}/v_t$

Fig. 5

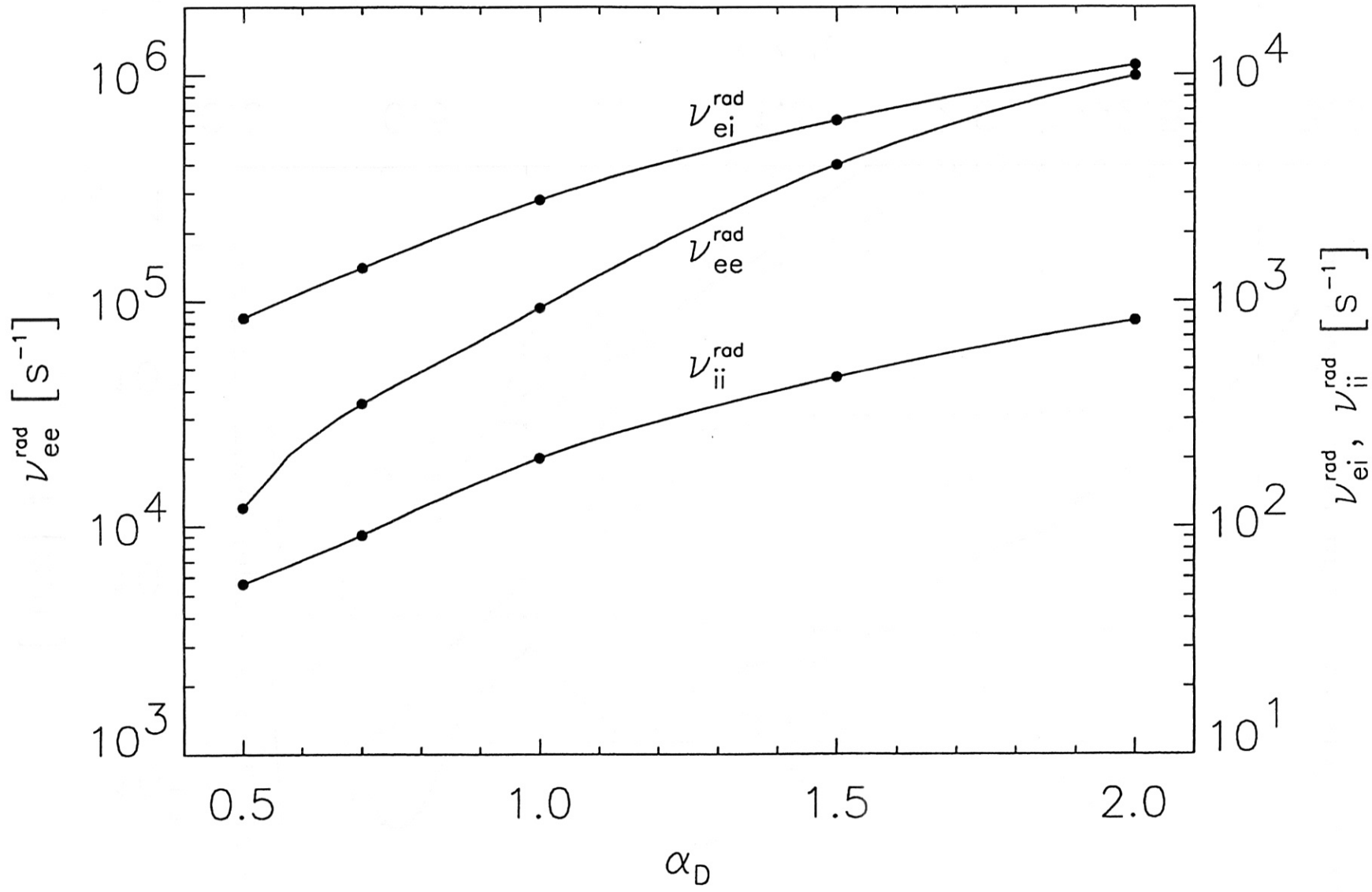
10^6
10^5
10^4
10^3
ν_{ee}^{rad} [s^{-1}]
ν_{ei}^{rad}
ν_{ee}^{rad}
ν_{ii}^{rad}
10^4
10^3
10^2
10^1
ν_{ei}^{rad}, ν_{ii}^{rad} [s^{-1}]
0.5
1.0
1.5
2.0
α_D

FIG. 6